Near-infrared absorbing pyrrolopyrrole aza-BODIPY-based donor-acceptor polymers with reasonable photoresponse

Feng, Ru
Department of Chemistry and Biochemistry, Graduate School of Engineering, Kyushu University

Sato, Narumi
Department of Chemistry and Biochemistry, Graduate School of Engineering, Kyushu University

Nomura, Mayuka
Department of Applied Chemistry, Graduate School of Engineering, Osaka University

Saeki, Akinori
Department of Applied Chemistry, Graduate School of Engineering, Osaka University

他

https://hdl.handle.net/2324/7179513

ARTICLE

Near-infrared absorbing pyrrolopyrrole aza-BODIPY-based donor-acceptor polymers with reasonable photoresponse †

Ru Feng,[a] Narumi Sato,[ab] Mayuka Nomura,[c] Akinori Saeki,[c] Hajime Nakanotani,[ad] Chihaya Adachi,[ad] Takuma Yasuda,[ab] Hiroyuki Furuta*[ae] and Soji Shimizu*[ae]

Designing near-infrared (NIR) absorbing donor-acceptor (D-A) polymers with photoresponse beyond 900 nm has remained a challenge in the area of organic photovoltaics (OPV) owing to the limited kinds of strong electron acceptors. Here we present the use of pyprrolopyrrole aza-BODIPY (PPAB) as a new acceptor group in D-A polymers in place of a conventional diketopyrrolopyrrole acceptor to achieve power conversion efficiencies up to 2.27% despite the ultra-small bandgap of 1.08 eV. The small photon energy loss of the PPAB-based D-A polymer and moderately high short-circuit current of 8.52 mA cm^{-2} arising from the panchromatic visible/NIR absorption guarantee PPAB as a potential building block of D-A polymers for NIR photovoltaics.

Introduction

Over the past two decades, semiconducting polymer-based bulk heterojunction (BHJ) photovoltaics[1,2] have emerged as a promising renewable energy technology owing to their advantages such as low cost, lightweight and solution-processing for flexible devices.[3,4] The certified power conversion efficiencies (PCEs) of such polymer solar cells (PSCs) have recently reached 14% by developing p- and n-type materials and device architectures and morphologies.[5] According to the Shockley-Queisser limit,[6] which predicts an optimal bandgap (E_g) of ~1.4 eV for a single-junction photovoltaic cell under AM1.5G 1 sun illumination, donor-acceptor (D-A) polymers exhibiting optical response up to ~900 nm have been intensively investigated,[2,7,8] thereby limiting the use of the rest of the solar spectrum in the near-infrared (NIR) region, which is indispensable for realizing multi-junction solar cells.[9,10]

Recently, Janssen *et al*. developed ultra-small bandgap D-A polymers with high NIR photoresponse (PCEs of 2.9–3.5% with up to 50% external quantum efficiency (EQE) at 1000 nm) by combining diketopyrrolopyrrole (DPP) as a conventional acceptor[7,11–15] with a series of strongly electron-donating

pyrrole-based groups, which progressively raise the HOMO level to decrease E_g to 1.13 eV.[16] Their pioneering work disclosed the crucial requisite for precise energy control of both p- and n-type materials to balance the photovoltaic performance and bandgap by minimizing energy loss (E_{loss}) defined by $E_g - eV_{oc}$, where e and V_{oc} denote the elementary charge and open-circuit voltage, respectively. The lower limit of E_{loss} has been proposed to be 0.6 eV due to the trade-off relationship with the quantum efficiency of charge generation.[17] E_{loss} of most successful PSCs thus ranges between 0.7 eV and 0.8 eV. Meanwhile, there have been reports on efficient charge generation in PSCs with E_{loss} less than 0.6 eV,[18] and further reduction of E_{loss} has recently been proposed to realize a new efficiency regime for organic photovoltaics (OPV).[19] In this context, although several factors should be considered, it is essential to tune the LUMO energy offset between p-type D-A polymers and n-type materials to minimize E_{loss} owing to the inherently small E_g for NIR PSCs.

Pyrrolopyrrole aza-BODIPY (PPAB)[20] is a newly designed functional chromophore derived from DPP and heteroaromatic amines by a facile Schiff base forming reaction.[21] Because of the π-extended structure, PPAB exhibits far-red/NIR absorption and fluorescence with high quantum yields, which have been further applied in various fields such as aggregation-induced emission enhancement (AIEE),[22] two-photon absorption (TPA),[23] photoacoustic imaging,[24,25] photothermal cancer therapy[25] and electrogenerated chemiluminescence (ECLs) in the NIR region.[26] During our investigation on OPV application of PPAB[20c] and PPAB-based small molecules,[27,28] we noticed that PPAB provides sufficiently deep LUMO levels for charge transfer to [6,6]-phenyl-C$_{71}$ butyric acid methyl ester (PC$_{71}$BM) acceptor. In the case of acceptor-donor-acceptor (A-D-A) triads using cyclopentadithiophene (CPDT) as a donor, the PCE was improved from DPP-CPDT-DPP triad (0.18%) to DPP-CPDT-PPAB triad (1.49%) and PPAB-CPDT-PPAB triad (3.88%) by

a. Department of Chemistry and Biochemistry, Graduate School of Engineering, Kyushu University, Fukuoka 819-0395, Japan
E-mail: hfuruta@cstf.kyushu-u.ac.jp, ssoji@cstf.kyushu-u.ac.jp
b. INAMORI Frontier Research Centre (IFRC), Kyushu University, Fukuoka 819-0395, Japan
c. Department of Applied Chemistry, Graduate School of Engineering, Osaka University, Suita 565-0871, Japan
d. Centre for Organic Photonics and Electronics Research (OPERA), Kyushu University, Fukuoka 819-0395, Japan
e. Centre for Molecular Systems (CMS), Kyushu University, Fukuoka 819-0395, Japan
†Electronic Supplementary Information (ESI) available: NMR and UV/vis/NIR absorption spectra, photovoltaic parameters and TEM images. See DOI: 10.1039/x0xx00000x
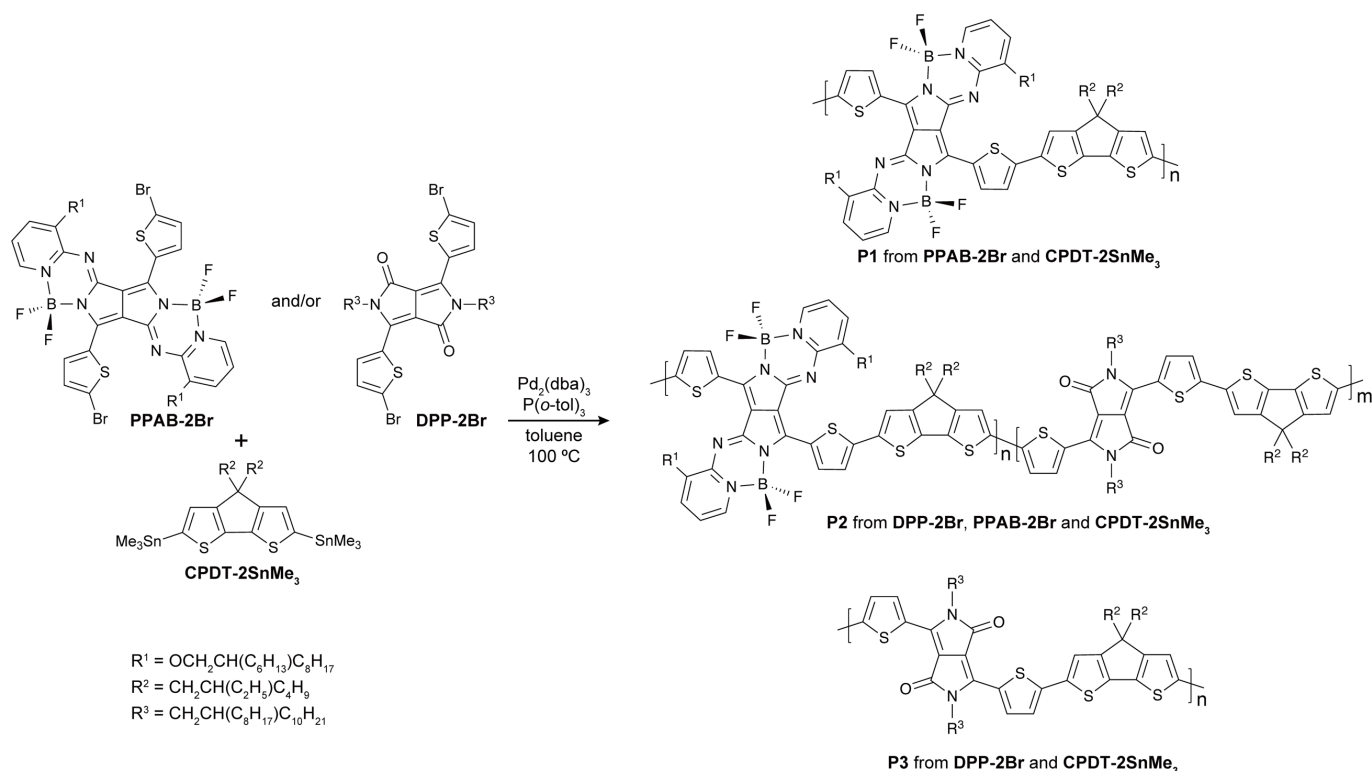
Scheme 1 Synthesis of DPP- and PPAB-based D-A polymers, **P1–P3**.

replacing a DPP acceptor with PPAB despite the gradual red-shift of the photoresponse up to 1000 nm in this order. In addition, the E_{loss} values of the PPAB-based triads (0.52 eV for DPP-CPDT-PPAB triad and 0.54 eV for PPAB-CPDT-PPAB triad) were smaller than the suggested lower limit.[17] These results motivated us to further extend PPAB-CPDT combination to the NIR PSCs.

To extend the library of the PPAB-based D-A polymers, here we present the synthesis of three kinds of D-A polymers comprising DPP or PPAB or both as acceptors and CPDT as a donor. Replacement of DPP with PPAB in the D-A polymers selectively lowered the LUMO level, while the HOMO level remained almost unchanged, decreasing E_g from 1.30 eV to 1.08 eV. Inversely, the PPAB-based PSCs showed better NIR photoresponse with PCEs up to 2.27% and a small E_{loss} value of 0.53 eV.

Results and discussion

Synthesis of DPP- and PPAB-based D-A polymers

The D-A polymers (**P1–P3**) were synthesized by palladium-catalyzed cross-coupling condensation polymerization[29] of dibromo-substituted DPP (**DPP-2Br**)[30] or PPAB (**PPAB-2Br**)[27] or both with bis(trimethylstannyl)-CPDT (**CPDT-2SnMe₃**)[31] (Scheme 1). All D-A polymers were purified by successive Soxhlet extraction with methanol, acetone, hexane and chloroform and obtained in high yields (77% for **P1**, 89% for **P2** and 79% for **P3**).[32]

Gel permeation chromatography (GPC) analysis in chloroform at 40 ⁰C revealed the number-average molecular

weights (M_n) of 45, 794 and 280 kg/mol for **P1**, **P2** and **P3** with rather high polydispersity index (PDI) of 67.4, 9.5 and 72.7, respectively, due to aggregation in chloroform, especially in the case of **P1** and **P3** (Table 1). The chemical structures of **P1–P3** were confirmed by ^{1}H NMR spectroscopy, which revealed the proton signals at similar chemical shifts to the corresponding triads reported in our previous study (Fig. S1–S3, ESI†).[28]

Optical and electrochemical properties

The optical and electrochemical properties of **P1–P3** were characterized by UV/vis/NIR absorption and photoelectron yield spectroscopies (PYS) (Table 1). In the film state, the D-A polymers exhibited intense, panchromatic absorption in the vis/NIR regions ranging from 300 to 1200 nm with an absorption maximum at 969, 912 and 816 nm for **P1**, **P2** and **P3**, respectively (Fig. 1). Introducing PPAB into the polymer backbone in place of DPP improved absorption in the shorter visible region and the NIR region. This trend agrees well with that observed for the PPAB- and/or DPP-based A-D-A triads in our previous study.[28] The red-shifts of the absorption spectra of these polymers by 162–665 cm^{-1} from the solution state to the thin film state were rather modest (Fig. S4, ESI†). The E_g estimated from the onset of the film absorption decreased in the order of **P3** (1.30 eV), **P2** (1.12 eV) and **P1** (1.08 eV) upon increasing the ratio of PPAB groups in the polymers. The PYS measurements revealed similar HOMO energy levels (**P1**: −5.19 eV, **P2**: −5.16 eV, and **P3**: −5.17 eV), indicating dominant contribution of the CPDT moiety to determine the HOMO energy levels of the polymers. On the basis of the E_g and the HOMO energy levels, the LUMO energy levels were

Table 1 Optical, electrochemical and polymer properties of **P1**, **P2** and **P3**

Compd.	$M_n{}^a$ (kg mol^{-1})	PDI^a	λ_{max}, solution^b (nm)	λ_{max}, film (nm)	HOMO^c (eV)	$E_g{}^d$ (eV)	LUMO^e (eV)
P1	45	67.4	954	969	−5.19	1.08	−4.11
P2	794	9.5	894	912	−5.16	1.12	−4.04
P3	280	72.7	774	816	−5.17	1.30	−3.87

^{a} Determined by GPC using polystyrene standards in chloroform as an eluent. ^{b} Chloroform solution. ^{c} Determined by PYS. ^{d} Determined from the onset of the film absorption. ^{e} HOMO + E_g

estimated to be −4.11 eV for **P1**, −4.04 eV for **P2** and −3.87 eV for **P3**. The LUMO energy levels decreased from **P3** to **P1** due to the stronger electron accepting nature of PPAB than DPP. Taken these results together, the ultra-small bandgaps of **P1**–**P3** (1.08–1.30 eV) were tuned mainly by the low lying LUMO energy levels of the PPAB groups.
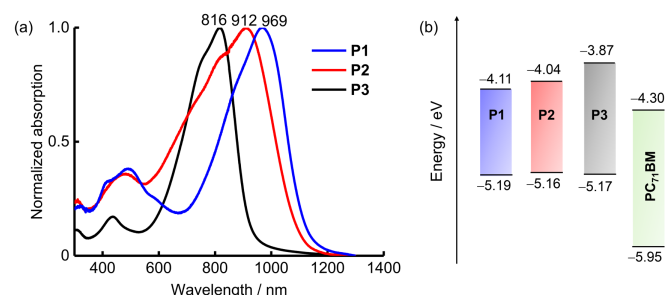

Fig. 1 (a) UV/vis/NIR absorption spectra of **P1** (blue), **P2** (red) and **P3** (black) in the thin film state. (b) Energy diagrams of the HOMO and LUMO of **P1**–**P3** and PC$_{71}$BM.

OPV performance

Time-resolved microwave conductivity (TRMC)[33–35] measurements using monochromatic light pulse from a nano-second laser (laser-flash)[36,37] or white-light pulse from a Xe flash-lamp (Xe-flash)[38] as the photoexcitation source provide the maximum transient conductivity ($\phi\Sigma\mu_{max}$) and photoconductivity maxima ($\Delta\sigma_{max}$), respectively. ϕ and $\Sigma\mu$ represent charge charrier generation efficiency and the sum of the hole and electron mobilities, whereas $\Delta\sigma_{max}$ includes information about not only the yield and local mobility of charge carriers, but also their lifetime and photoabsorption. The increase in $\phi\Sigma\mu_{max}$ upon mixing **P1**–**P3** with [6,6]-phenyl-C$_{61}$ butyric acid methyl ester (PC$_{61}$BM) indicated that all polymers can function as a p-type material in BHJ-OPVs (Fig. S5a, ESI†). On the basis of $\Delta\sigma_{max}$, the best ratio of polymers and PC$_{61}$BM was estimated to lie between 1:1 and 1:2, and the magnitude of $\Delta\sigma_{max}$ was in the order of **P1** > **P2** > **P3** (Fig. S5b, ESI†).

To improve photoresponse in the visible region, PC$_{71}$BM was used instead of PC$_{61}$BM, and BHJ-OPVs with an inverted device structure of indium tin oxide (ITO)/ZnO (30 nm)/**P1**–**P3**:PC$_{71}$BM (36−134 nm)/MoO$_3$ (10 nm)/Ag (100 nm) were fabricated (Fig. S6, ESI†). The potential device conditions according to the TRMC measurements were further optimized by controlling polymers/PC$_{71}$BM ratio, active-layer thickness and amount of solvent additives as described in detail below.

Considering the low solubility of **P1**, chlorobenzene was selected as a solvent for device fabrication owing to the better

solubility at high temperature. After screening the D/A ratio from 1:1 to 1:3 according to the TRMC measurements, the optimal D/A ratio of polymers and PC$_{71}$BM for BHJ-OPVs was 1:1 for **P1** and **P2** and 1:3 for **P3** (Fig. S7, S11 and S14 and Tables S1, S5 and S8, ESI†). Among various additives tested (1,8-diiodooctane (DIO), 1-chloronaphthalene (CN) and diphenyl ether (DPE)), **P1**-based PSCs processed with DPE exhibited the highest PCE of 2.27% compared with those with other additives (PCEs of 2.13% and 1.78% using DIO and CN as an additive, respectively) (Fig. S8 and Table S2, ESI†). The optimal amount of DPE additive varies depending on polymers, 0.5% for **P1**, 2.5% for **P2** and 1.0% for **P3** (Fig. S9, S12 and S15 and Tables S3, S6 and S9, ESI†). For the active layer thickness, the polymers exhibited the best OPV performance when the thickness is less than 70 nm (61 nm for **P1**, 68 nm for **P2** and 69 nm for **P3**) (Fig. S10, S13 and S16 and Tables S4, S7 and S10, ESI†).
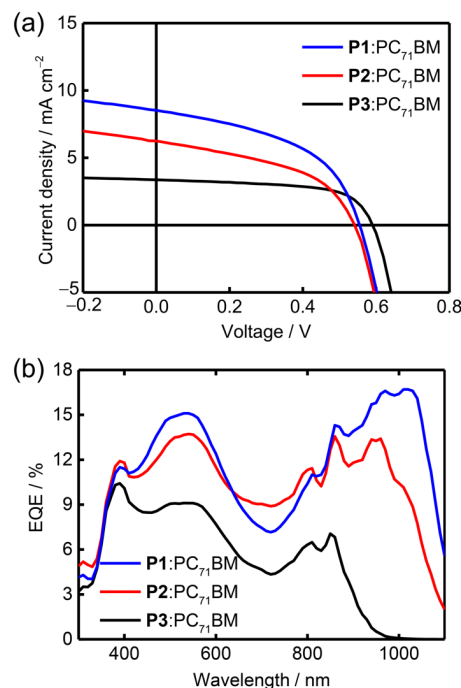

Fig. 2 (a) *J*–*V* curves and (b) EQE spectra of **P1**–**P3**:PC$_{71}$BM BHJ-OPVs.

The fill factor (FF) of **P1**-based PSCs decreased as the thickness was increased from 36 to 100 nm due to the lowering of the extraction efficiency of photogenerated carriers, whereas the J_{sc} was enhanced to a certain degree. A closer look at the changes in the external quantum efficiency (EQE) spectra of **P1**-based PSCs at various thicknesses revealed the increase

Table 2 Device characteristics of **P1**–**P3**:PC$_{71}$BM BHJ-OPVs

Active layer (p/n ratio)	Thickness (nm)	J_{sc} (mA cm^{-2})	V_{oc} (V)	FF	PCE (%)	EQE$_{max}$	E_{loss}[a] (eV)
P1:PC$_{71}$BM (1:1)	61	8.52	0.55	0.48	2.27	0.17	0.53
P2:PC$_{71}$BM (1:1)	69	6.25	0.54	0.46	1.56	0.14	0.58
P3:PC$_{71}$BM (1:3)	69	3.36	0.59	0.62	1.23	0.07	0.71

[a] $E_{loss} = E_g - eV_{oc}$
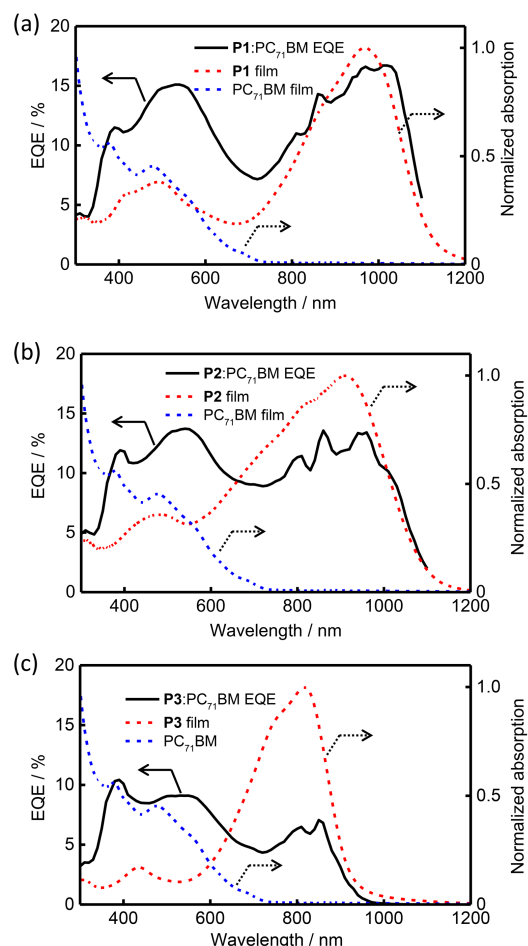
Fig. 3 EQE spectra of the optimized PSC of (a) **P1**, (b) **P2** and (c) **P3** superimposed on the UV/vis/NIR absorption spectra of the corresponding polymers and PC$_{71}$BM in the film state.

in EQE in the NIR region when the thickness was increased up to 61 nm owing to the NIR photoresponse of **P1**, whereas the EQE in the visible region dropped at larger thicknesses (~100 nm) due to the aggregation of PC$_{71}$BM. A similar tendency was observed for **P3**-based PSCs. In contrast, the EQE spectra of **P2**-based PSCs decreased in the whole vis/NIR regions at the high thicknesses due to poor charge transportation.

The current density-voltage (*J*–*V*) characteristics and EQE spectra of the optimized devices for **P1**–**P3** are shown in Fig. 2, and the data are summarized in Table 2. Because of the longer wavelength limit of our instrument, the EQE spectra ended at 1100 nm. As anticipated from the HOMO energy levels (Table 1), similar V_{oc} of 0.54–0.59 V was observed for all the PSCs. In contrast, the short-circuit current (J_{sc}) increased from **P3** (3.36 mA cm^{-2}) to **P2** (6.25 mA cm^{-2}) and further to **P1** (8.52 mA cm^{-2}). The high J_{sc} of **P1**-based PSCs can be attributed to the intense,

panchromatic absorption of **P1** compared with **P2** and **P3**. The order of J_{sc} as well as PCE are consistent with that of $\Delta\sigma_{max}$ obtained in the TRMC measurements using a white-light pulse. The EQE spectra of the optimized devices, which were superimposed on the absorption spectra of the corresponding polymers and PC$_{71}$BM, ensured NIR photoresponse of **P1** and **P2** extending to 1200 nm (Fig. 3).

To rationalize the high PCE of 2.27% and NIR photoresponse in the case of the **P1**-based PSC, maximum EQE (EQE$_{max}$) and E_{loss} values were compared (Table 2). In inverse proportion to the decrease of E_{loss} values from **P3** (0.71 eV) to **P2** (0.58 eV) and **P1** (0.52 eV), the EQE$_{max}$ increased from **P3** (7%) to **P2** (14%) and **P1** (17%). It is remarkable that the E_{loss} values of **P1** and **P2** are below the empirical lower limit of 0.6 eV.[17] This indicates that PPAB-based polymers are highly compatible with fullerene-based acceptors, although several mechanisms should be incorporated into the working mechanism with the low E_{loss} for the **P1**- and **P2**-based PSCs.

Film morphology

The transmission electron microscopy (TEM) was used for further study on the interior morphologies of the BHJ active
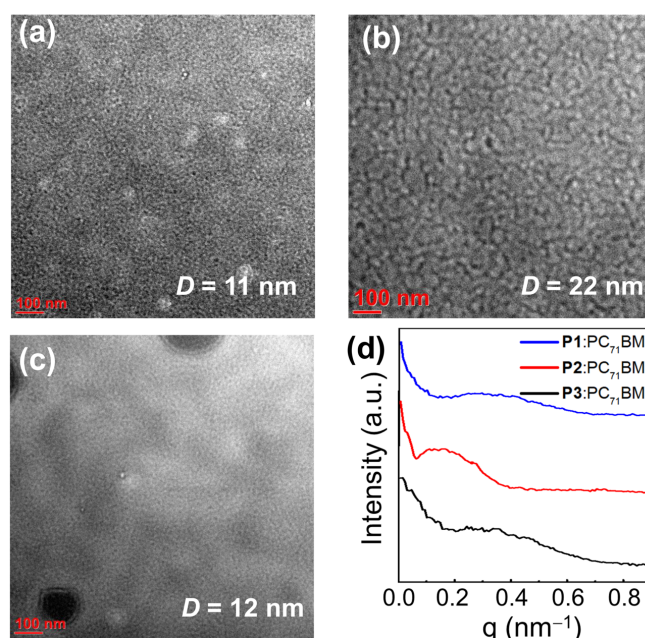
Fig. 4 TEM images of BHJ active layers composed of (a) **P1**:PC$_{71}$BM (1:1 (w/w)), (b) **P2**:PC$_{71}$BM (1:1 (w/w)) and (c) **P3**:PC$_{71}$BM (1:3 (w/w)) blends. The *D* values represent the average domain sizes. (d) Power spectral density profiles of the blend films obtained from the radially averaged 2D-FFT analysis of the TEM images.

layers to reveal the difference in nanoscale phase segregation of **P1**–**P3** (Fig. 4).

The bright and dark regions represented the polymer-rich and $PC_{71}BM$-rich domains, respectively, due to the higher electron density of $PC_{71}BM$ than that of polymers. All the active layers exhibited homogeneous and fine nanostructures with different domain sizes. The domain sizes (*D*) estimated using power spectral densities (PSDs) calculated by the two-dimensional fast Fourier transform (2D FFT) analysis were 11 nm for **P1**:$PC_{71}BM$, 22 nm for **P2**:$PC_{71}BM$ and 12 nm for **P3**:$PC_{71}BM$.[39] Considering the short exciton diffusion length of organic semiconductor, which is normally less than 10 nm, the small *D* of **P1**:$PC_{71}BM$ may facilitate charge generation at the D/A interfaces to attain high J_{sc} values. In addition to the small E_{loss}, the suitable *D* of **P1**:$PC_{71}BM$ also contributes to its reasonable photoresponse in the NIR region.

Conclusions

In this study, we have developed a series of D-A polymers comprising DPP or PPAB or both as acceptors. Upon replacement of DPP with PPAB, the optical bandgap decreased from 1.30 eV to 1.08 eV due to the stronger electron accepting nature of PPAB than DPP. Consequently, panchromatic absorptions extending to 1200 nm were achieved for the PPAB-based polymers (**P1** and **P2**). Despite the small E_{loss} values below 0.6 eV, which generally causes inefficient charge generation, PPAB-based PSCs with $PC_{71}BM$ as a n-type material exhibited moderately high NIR photoresponse with EQE_{max} of 17% for **P1** and 14% for **P2**. Ultimately, the best performance with PCE of 2.27% and the J_{sc} as high as 8.52 mA cm^{-2} was achieved for the **P1**-based PSC. Considering the D-A polymers with NIR photoresponse have still been on its infant stage, the small E_{loss} of PPAB-based polymers in combination with $PC_{71}BM$ is highly potential for future application in the NIR PSCs. In addition, further improvement of photoresponse in the visible region by controlling the HOMO energy level with other types of donor groups in place of CPDT may enhance the overall PCEs. Research along these directions will be reported in due course from our laboratory.

Experimental

Instrumentation and measurements

Electronic absorption spectra were recorded on a JASCO V-770 spectrophotometer. ^{1}H NMR spectra were recorded on a JEOL JNM-ECX500 spectrometer (operating at 495 MHz for ^{1}H) using a residual solvent as an internal reference for [1]H (δ = 7.26 ppm for $CDCl_3$). Molecular weights (number-average molecular weight: M_w) and polydispersity index (PDI) of polymers were determined using a size exclusion chromatography (SEC) (gel permeation chromatography: GPC) method with polystyrene standards. SEC-GPC analysis was performed using chloroform as an eluent at a flow rate of 1 cm^3 min^{-1} at 40 °C, on a SHIMADZU LC-20AT/CBM-20A/CTO-20A chromatography instrument connected to a SHIMADZU SPD-M20A UV/vis detector. Photoelectron yield spectra (PYS) were recorded on a RikenKeiki AC-3 ultraviolet photoelectron spectrometer. Transmission

electron microscopy (TEM) images were obtained using a JEM-2010 transmission electron microscope (JEOL) at an accelerating voltage of 120 keV. The spin-coated thin films on mica were peeled from substrates by soaking in water and then transferred onto copper grids for TEM observations. All reagents and solvents used for reactions were of commercial reagent grade and were used without further purification unless noted otherwise. All solvents used in optical measurements were of commercial spectroscopic grade.

Time-resolved microwave conductivity (TRMC)

A resonance cavity was used to obtain a high degree of sensitivity in the conductivity measurement. The resonance frequency and microwave power were set at ca. 9.1 GHz and 3 mW, respectively, so that the electric field of the microwave was sufficiently small not to disturb the motion of charge carriers. Nanosecond laser pulse at third-harmonic generation (THG; 355 nm) of a Nd:YAG laser (Continuum, Surelite II, 5–8 ns pulse duration, 10 Hz) or microsecond white-light pulse from a Xe flash lamp was used as an excitation source. The photoconductivity $\Delta\sigma$ was obtained by $\Delta P_r/(AP_r)$ where ΔP_r, A and P_r are the transient power changes of the reflected microwave from a cavity, the sensitivity factor and the reflected microwave power, respectively. The power of the white-light pulse was 0.3 mJ cm^{-2} $pulse^{-1}$. The samples were drop-cast on a quartz plate from solutions of the polymers and $PC_{61}BM$ and dried in a vacuum oven. The TRMC experiments were performed under ambient conditions at room temperature.

OPV device fabrication and evaluation

Prepatterned ITO-coated glass substrates were ultrasonic cleaned sequentially in detergent solution (15 min), deionized water (10 min × 2) and acetone (10 min), kept in isopropyl alcohol overnight, and then subjected to UV/ozone treatment for 30 min. A thin layer (~30 nm) of ZnO was prepared by spin-coating (at 5000 rpm for 30 s) a precursor solution of zinc acetate (1.00 g) and ethanolamine (0.28 g) in 2-methoxyethanol (10 mL) filtered through a 0.45 μm poly(tetrafluoroethylene) membrane filter, followed by baking at 200 °C for 10 min under air. The photoactive layer was then deposited by spin-coating from a chlorobenzene solution containing a donor and $PC_{71}BM$ after passing through a 0.45 μm poly(tetrafluoroethylene) membrane filter. The thicknesses of the photoactive layers were ca. 36–134 nm, measured with a profilometer. The thin films were then loaded into an E-200 vacuum evaporation system (ALS Technology). Finally, 10-nm-thick MoO_3 and 100-nm-thick Ag layers were sequentially vacuum-deposited on top of the photoactive layers under high vacuum (<5.0 × 10^{-4} Pa) through a shadow mask, defining an active area of 0.04 cm^2 for each device. The current density–voltage (*J–V*) characteristics and EQE spectra of the fabricated OPVs were measured with a computer-controlled Keithley 2400 source measure unit in air, under simulated AM 1.5G solar illumination at 100 mW cm^{-2} (1 sun) conditions, using a Xe lamp-based SRO-25GD solar simulator and IPCE measurement system (Bunko Keiki). The light intensity was calibrated using a certified silicon photovoltaic reference cell.

Synthesis

P1: **PPAB-2Br** (119 mg, 0.10 mmol) and **CPDT-2SnMe₃** (73 mg, 0.10 mmol), Pd$_2$(dba)$_3$ (2.75 mg, 0.003 mmol) and P(*o*-tol)$_3$ (4.56 mg, 0.015 mmol) were dissolved in dry toluene (6 mL). After degassing three times by freeze–pump–thaw cycles, the mixture was stirred for 48 h at 100 °C. After cooling to room temperature, the reaction mixture was poured into methanol and stirred for 0.5 h at room temperature. After filtration, the product was subjected to Soxhlet extraction using methanol, acetone, hexane and chloroform to afford **P1** as a black solid (110 mg, 77%).

P2: The same synthetic and purification procedures as with **P1** were applied to a mixture of **DPP-2Br** (51 mg, 0.05 mmol), **PPAB-2Br** (59 mg, 0.05 mmol), **CPDT-2SnMe₃** (73 mg, 0.10 mmol), Pd$_2$(dba)$_3$ (2.75 mg, 0.003 mmol) and P(*o*-tol)$_3$ (4.56 mg, 0.015 mmol). **P2** was obtained as a black solid (120 mg, 89%).

P3: The same synthetic and purification procedures as with **P1** were applied to a mixture of **DPP-2Br** (102 mg, 0.10 mmol), **CPDT-2SnMe₃** (73 mg, 0.10 mmol), Pd$_2$(dba)$_3$ (2.75 mg, 0.003 mmol) and P(*o*-tol)$_3$ (4.56 mg, 0.015 mmol). **P3** was obtained as a black solid (100 mg, 79%).

Conflicts of interest

There are no conflicts to declare.

Acknowledgements

Notes and references

1   Y. Huang, E. J. Kramer, A. J. Heeger and G. C. Bazan, *Chem. Rev.*, 2014, **114**, 7006.
2   (a) G. Li, R. Zhu and Y. Yang, *Nat. Photonics*, 2012, **6**, 153; (b) L. Dou, Y. Liu, Z. Hong, G. Li and Y. Yang, *Chem. Rev.*, 2015, **115**, 12633.
3   M. Kaltenbrunner, M. S. White, E. D. Głowacki, T. Sekitani, T. Someya, N. S. Sariciftci and S. Bauer, *Nat. Commun.*, 2012, **3**, 770.
4   R. Søndergaard, M. Hösel, D. Angmo, T. T. Larsen-Olsen and F. C. Krebs, *Mater. Today*, 2012, **15**, 36.
5   (a) S. Zhang, Y. Qin, J. Zhu and J. Hou, *Adv. Mater.*, 2018, **30**, 1800868; (b) Z. Zheng, Q. Hu, S. Zhang, D. Zhang, J. Wang, S. Xie, R. Wang, Y. Qin, W. Li, L. Hong, N. Liang, F. Liu, Y. Zhang, Z. Wei, Z. Tang, T. P. Russell, J. Hou and H. Zhou, *Adv. Mater.*, 2018, **30**, 1801801; (c) S. Li, L. Ye, W. Zhao, H. Yan, B. Yang, D. Liu, W. Li, H. Ade and J. Hou, *J. Am. Chem. Soc.*, 2018, **140**, 7159.
6   W. Shockley and H. J. Queisser, *J. Appl. Phys.*, 1961, **32**, 510.
7   W. Li, K. H. Hendriks, M. M. Wienk and R. A. J. Janssen, *Acc. Chem. Res.*, 2016, **49**, 78.
8   J. W. Jung, J. W. Jo, E. H. Jung and W. H. Jo, *Org. Electron.*, 2016, **31**, 149.
9   (a) D. Di Carlo Rasi and R. A. J. Janssen, *Adv. Mater.*, 2018, **31**, 1806499; (b) W. Li, A. Furlan, K. H. Hendriks, M. M. Wienk and R. A. J. Janssen, *J. Am. Chem. Soc.*, 2013, **135**, 5529.
10 G. Li, W.-H. Chang and Y. Yang, *Nat. Rev. Mater.*, 2017, **2**, 17043.
11 (a) M. Li, A. H. Balawi, P. J. Leenaers, L. Ning, G. H. L. Heintges, T. Marszalek, W. Pisula, M. M. Wienk, S. C. J. Meskers, Y. Yi, F. Laquai and R. A. J. Janssen, *Nat. Commun.*, 2019, **10**, 2867; (b) G. H. L. Heintges and R. A. J. Janssen, *RSC Advances*, 2019, **9**, 15703.
12 S. Qu and H. Tian, *Chem. Commun.*, 2012, **48**, 3039.
13 G. Oklem, X. Song, L. Toppare, D. Baran and G. Gunbas, *J. Mater. Chem. C*, 2018, **6**, 2957.
14 M. Grzybowski and D. T. Gryko, *Adv. Optical Mater.*, 2015, **3**, 280.
15 (a) W. Shin, T. Yasuda, Y. Hidaka, G. Watanabe, R. Arai, K. Nasu, T. Yamaguchi, W. Murakami, K. Makita and C. Adachi, *Adv. Energy Mater.*, 2014, **4**, 1400879; (b) W. Shin, T. Yasuda, G. Watanabe, Y. S. Yang and C. Adachi, *Chem. Mater.*, 2013, **25**, 2549.
16 K. H. Hendriks, W. Li, M. M. Wienk and R. A. J. Janssen, *J. Am. Chem. Soc.*, 2014, **136**, 12130.
17 D. Veldman, S. C. J. Meskers and R. A. J. Janssen, *Adv. Funct. Mater.*, 2009, **19**, 1939.
18 (a) W. Li, K. H. Hendriks, A. Furlan, M. M. Wienk and R. A. J. Janssen, *J. Am. Chem. Soc.*, 2015, **137**, 2231; (b) X. Long, Z. Ding, C. Dou, J. Zhang, J. Liu and L. Wang, *Adv. Mater.*, 2016, **28**, 6504; (c) Y. Wang, Q. Fan, X. Guo, W. Li, B. Guo, W. Su, X. Ou and M. Zhang, *J. Mater. Chem. A*, 2017, **5**, 22180; (d) P. Cheng, M. Zhang, T.-K. Lau, Y. Wu, B. Jia, J. Wang, C. Yan, M. Qin, X. Lu and X. Zhan, *Adv. Mater.*, 2017, **29**, 1605216.
19 S. M. Menke, N. A. Ran, G. C. Bazan and R. H. Friend, *Joule*, 2018, **2**, 25.
20 (a) S. Shimizu, *Chem. Commun.*, 2019, **55**, 8722; (b) S. Shimizu, T. Iino, Y. Araki and N. Kobayashi, *Chem. Commun.*, 2013, **49**, 1621; (c) S. Shimizu, T. Iino, A. Saeki, S. Seki and N. Kobayashi, *Chem. – Eur. J.*, 2015, **21**, 2893.
21 (a) S. Shimizu, A. Murayama, T. Haruyama, T. Iino, S. Mori, H. Furuta and N. Kobayashi, *Chem. – Eur. J.*, 2015, **21**, 12996; (b) M. Tamada, T. Iino, Y. Wang, M. Ide, A. Saeki, H. Furuta, N. Kobayashi and S. Shimizu, *Tetrahedron Lett.*, 2017, **58**, 3151; (c) M. Fukuda, S. Mori, H. Furuta and S. Shimizu, *Chem. – Asian. J.*, 2019, **14**, 1697.
22 L. Li, L. Wang, H. Tang and D. Cao, *Chem. Commun.*, 2017, **53**, 8352.
23 Y. Zhou, C. Ma, N. Gao, Q. Wang, P.-C. Lo, K. S. Wong, Q.-H. Xu, T. Kinoshita and D. K. P. Ng, *J. Mater. Chem. B*, 2018, **6**, 5570.
24 K. Miki, A. Enomoto, T. Inoue, T. Nabeshima, S. Saino, S. Shimizu, H. Matsuoka and K. Ohe, *Biomacromolecules*, 2017, **18**, 249.
25 C. Wu, X. Huang, Y. Tang, W. Xiao, L. Sun, J. Shao and X. Dong, *Chem. Commun.*, 2019, **55**, 790.
26 R. Ishimatsu, H. Shintaku, Y. Kage, M. Kamioka, S. Shimizu, K. Nakano, H. Furuta and T. Imato, *J. Am. Chem. Soc.*, 2019, **141**, 11791.
27 Y. Kage, S. Mori, M. Ide, A. Saeki, H. Furuta and S. Shimizu, *Mater. Chem. Front.*, 2018, **2**, 112.
28 R. Feng, N. Sato, T. Yasuda, H. Furuta and S. Shimizu, *Chem. Commun.*, 2020, **56**, 2975.
29 H.-Y. Chen, M. Nikolka, A. Wadsworth, W. Yue, A. Onwubiko, M. Xiao, A. J. P. White, D. Baran, H. Sirringhaus and I. McCulloch, *Macromolecules*, 2018, **51**, 71.
30 J. Yu, B. Zhao, X. Nie, B. Zhou, Y. Li, J. Hai, E. Zhu, H. Bian, H. Wu and W. Tang, *New J. Chem.*, 2015, **39**, 2248.
31 A. Rana, Y. Hong, T. Y. Gopalakrishna, H. Phan, T. S. Herng, P. Yadav, J. Ding, D. Kim and J. Wu, *Angew. Chem. Int. Ed.*, 2018, **57**, 12534.

32 Polymers, **P1**–**P3**, are photo- and thermally stable in solution, thin film and solid states under the purification and device fabrication conditions.

33 A. Saeki, Y. Koizumi, T. Aida and S. Seki, *Acc. Chem. Res.*, 2012, **45**, 1193.

34 F. C. Grozema and L. D. A. Siebbeles, *J. Phys. Chem. Lett.*, 2011, **2**, 2951.

35 T. J. Savenije, J. E. Kroeze, X. Yang and J. Loos, *Adv. Funct. Mater.*, 2005, **15**, 1260.

36 (a) W. Zhang, W. Jin, T. Fukushima, A. Saeki, S. Seki and T. Aida, *Science*, 2011, **334**, 340; (b) A. Saeki, M. Tsuji and S. Seki, *Adv. Energy Mater.*, 2011, **1**, 661.

37 (a) A. M. Nardes, A. J. Ferguson, J. B. Whitaker, B. W. Larson, R. E. Larsen, K. Maturová, P. A. Graf, O. V. Boltalina, S. H. Strauss and N. Kopidakis, *Adv. Funct. Mater.*, 2012, **22**, 4115; (b) A. J. Ferguson, N. Kopidakis, S. E. Shaheen and G. Rumbles, *J. Phys. Chem. C*, 2008, **112**, 9865.

38 A. Saeki, S. Yoshikawa, M. Tsuji, Y. Koizumi, M. Ide, C. Vijayakumar and S. Seki, *J. Am. Chem. Soc.*, 2012, **134**, 19035.

39 (a) W. Ma, C. Yang and A. J. Heeger, *Adv. Mater.*, 2007, **19**, 1387; (b) J. S. Moon, J. K. Lee, S. Cho, J. Byun and A. J. Heeger, *Nano Lett.*, 2009, **9**, 230.